

Marco Antonio Muraro

marco_dylan@hotmail.com
Federal University of Technology – Paraná
Mechanical & Materials Engineering Postgraduate
Program (PPGEM-UTFPR)
80230-901 Curitiba, Paraná, Brazil

Fábio Koda

fabiokoda@yahoo.com.br
Cia Paranaense de Energia (COPEL)
Distribution Department
80420-170 Curitiba, Paraná, Brazil

Urbano Reisdorfer Jr.

ureisdorfer@hotmail.com
Federal University of Technology – Paraná
Mechanical Academic Department (DAMEC)
80230-901 Curitiba, Paraná, Brazil

Carlos Henrique da Silva

carloschs@utfpr.edu.br
Federal University of Technology – Paraná
Mechanical & Materials Engineering Postgraduate
Program (PPGEM-UTFPR)
80230-901 Curitiba, Paraná, Brazil

The Influence of Contact Stress Distribution and Specific Film Thickness on the Wear of Spur Gears During Pitting Tests

One of the main gear damage mechanisms is the formation of pitting and spalling on the tooth flank. Several factors have significant influence on the damage formation, such as: contact stress level; tooth profile type; relative contact speed; surface finish and lubrication conditions. This work comprehends the global observation of all such parameters and was carried out to explain the phenomena related to this wear mechanism. The wear test equipment uses the power recirculation principle and is commonly known as FZG test rig. The gears were made from AISI 8620 steel and had two types of surface finishing (by shaving or by milling). The wear experiments were performed with two torque stages: 135 N.m (running-in) and 302 N.m (steady-state), and two test temperatures: 60°C (running-in) and 90°C (steady-state). The wear level was determined by using image analysis. In order to calculate the specific film thickness and friction coefficient, the roughness of tooth flank was measured at each test stop. After the experiments were completed, it was possible to confirm that, for both manufacturing processes, the boundary lubrication regime was adopted at the tooth flank and the specific film thickness presents a different behavior when compared to addendum, pitch diameter and dedendum regions. The wear on the gear flanks depended on the lubricant film thickness and it was higher for the milled gears.

Keywords: contact fatigue, gears, pitting, shaving, contact stress, specific film thickness

Introduction

There are basically two gear teeth failure modes: bending fatigue at the teeth root and contact (or surface) fatigue at the teeth flank. The contact fatigue is caused by the stresses developed at the region of contact between the teeth flanks, which, after several cycles, will lead to crack initiation. The contact conditions are responsible for the nucleation of these cracks on the surface or sub-surface of the teeth flanks. The cracks propagation may result in failure by pitting and/or spalling (Cheng, 1983).

The contact stresses on non-conformal surfaces, such as in gears, can be estimated by analytical equations based on the elasticity theory developed by Hertz in 1881 (Stachowiak and Batchelor, 2005). In this case, the contact between two teeth is usually compared to the contact between two equivalent cylinders with the radii identical to the flanks' radii curvatures in the contact point. It is very important to find which parameters of the tribological system affect the Hertzian stress levels along the contact action line. Among the main influence factors it can be mentioned: the geometric profile of the tooth flank (modulus, number of teeth, pressure angle), the gear materials, the lubricant properties, the load transmitted and the kinematics of the movement.

The surface finishing has a strong influence on the gear life, and the roughness behaves as a stress concentration factor for crack initiation; therefore, this is a relevant issue when analyzing the gear flanks wear. Several studies have been conducted to verify the roughness effect on the resistance to contact fatigue. According to Zafosnik et al. (2007), at the rolling and sliding contact, the resistance to fatigue depends on different factors, such as stress and elastoplastic strain, material properties, physicochemical properties of lubricant, surface roughness, residual stress and contact kinematics. The surface cracks could be initiated near the deformed

surface zone, in the region of maximum cyclic shear stress caused by rolling-sliding contact or, alternatively, near defects such as notches or scratches.

The load sharing function defines the load distribution profile along the gear contact. The use of this function is important to identify which tooth regions will be fully supporting the efforts transmitted. Figure 1 shows the two main load sharing forms.

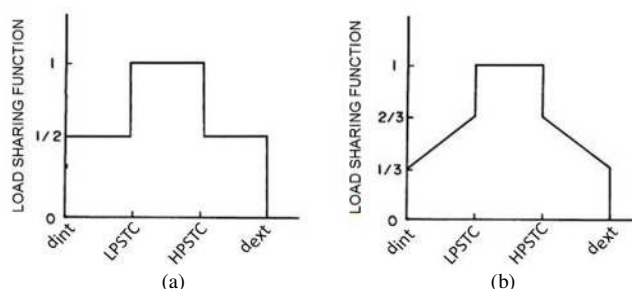


Figure 1. Load-sharing function versus pinion roll angle: (a) instantaneous mode, (b) influenced by the lubricant and deformation in the tooth. (Adapted from ASM, 1992).

It is known that from the gear LPSTC (lowest point of single tooth contact) to the HPSTC (highest point of single tooth contact), there is only a geared pair, that is, regardless of the load sharing function used, the normal force for this region will always be equal to the maximum normal force. Below the LPSTC and above the HPSTC there is more than one pair in contact.

Therefore, the load sharing function becomes important to determine such forces. Figure 2 illustrates the LPSTC and HPSTC points for a gear tooth and the regions where the load sharing function - $f(d)$ - will take place.

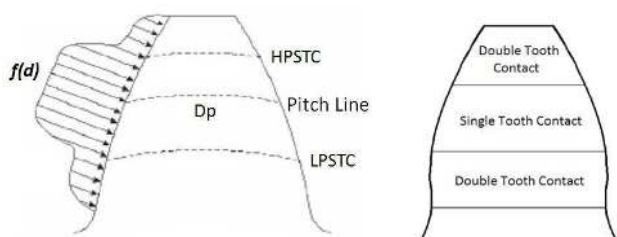


Figure 2. Schematic pictures of LPSTC, HPSTC, pitch line and load sharing function - $f(d)$ (Adapted from Imrek, 2009).

As shown in Fig. 3, three steps are identified in the gear movement kinematics. At the beginning, the contact occurs through a combination of rolling and sliding (friction) between the teeth. In the pitch diameter region there is simple rolling, and after this point, sliding and rolling will occur again.

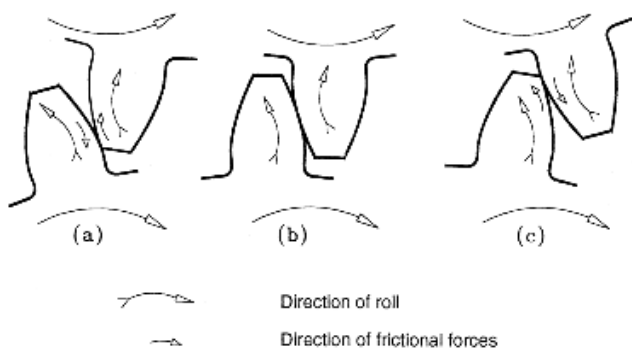


Figure 3. Mechanics of gear tooth contact: (a) at point of first contact; (b) at pitch point and (c) at last point of contact (Adapted from Walton and Goodwin, 1988).

The friction force provokes changes in the stress field generated by the contact between bodies, thus exerting great influence on the contact fatigue failure. Among the friction models that describe the friction coefficient for gears in contact, emphasis should be given to (i) the DIN 3990 (1987) equation; (ii) the equation described in ISO 6336 (1996); (iii) the model proposed by Michaelis (Winter and Michaelis, 1983); (iv) the Kelly expression, and (v) an equation for FZG gears proposed by Castro (2004). It is known from studies conducted by Honh (2004) that friction is also greatly influenced by the additive types present in the lubricants. Another important factor mentioned by Honh is related to the gears coating. Therefore, it can be stated that the proposed models may show some changes when working with gears coated with fortified lubricants.

Lubrication is aimed at introducing a low shear strength film, which ends up weakening the resistance of these joints, and thus reducing friction. In some cases, the lubricant may not fully prevent contact between the asperities, although it may reduce the severity of contact conditions. In other situations, the lubricant separates the surfaces completely, and joints with asperities are not formed. Thus, to a greater or lesser extent, the use of lubricants will always reduce the wear rate, and this will be a direct function of this type of lubrication. There are basically three different lubrication regimes: hydrodynamic (HD), elasto-hydrodynamic (EHD) and boundary lubrication. In many cases, a mixed lubrication condition refers to the intermediate regime between EHD and boundary lubrication.

The contact between the gear teeth surfaces is "non-conformal", i.e., it nominally (under zero load) involves a line or point of contact, generating small-area concentrated contacts. Under these

conditions, elasto-hydrodynamic (EHD) is the predominant lubrication regime. Whenever the oil film breaks, the lubrication regime turns into boundary lubrication, where almost the entire load is supported by the asperities (Grubin, 1949).

The specific film thickness (λ) determines the lubrication conditions. This parameter depends only on the minimum lubrication film thickness and surface roughness. For $\lambda > 3$, a full fluid lubricant film separates the two surfaces; the contact between asperities is negligible, and both the friction and the wear should be very low. However, several non-conformal contacts operate with $\lambda < 3$. For $1 < \lambda < 3$, the lubrication condition is partial or mixed EHD. Under these conditions, some contact between the asperities will occur, and the wear will be greater than in conditions where a full fluid lubricant film is present (Hutchings, 1992).

The main objective of this work is monitoring changes in the contact conditions (Hertzian pressures, specific film thickness and friction coefficient) along the mesh while testing the contact fatigue of spur gears made from AISI 8620 hardened steel, with two different kinds of surface finishing: shaving and milling.

Nomenclature

b	= face gear width, mm
d_1	= pinion pitch diameter, mm
d_{int}	= internal diameter, mm
d_{ext}	= external diameter, mm
E	= Young modulus, GPa
E'	= effective Young modulus, GPa
EHD	= elasto-hydrodynamic lubrication
$f(d)$	= load sharing function, N
FZG	= Forschungsstelle für Zahnräder und Getriebebau
HD	= hydrodynamic lubrication
h_{min}	= minimum film thickness, mm
HPSTC	= highest point of single tooth contact
LPSTC	= lowest point of single tooth contact
m	= module, mm
p_{max}	= maximum contact pressure, MPa
R	= radius of curvature at the contact point, mm
R'_{eq}	= equivalent radius of curvature at contact point, mm
R_a	= arithmetic average roughness, μm
R_{aEq}	= equivalent arithmetic average roughness, μm
R_q	= root mean square roughness, μm
R_{sm}	= mean spacing at mean line, mm
R_{vk}	= depth of valleys in Abbott-Firestone curve, μm
T	= Torque, N.m
U	= average velocity, m/s
V	= tangential speed, m/s
V_R	= rolling speed, m/s
W	= normal load, N
W_L	= specific normal load, N/m
X_C	= correction for coated gears, dimensionless
X_L	= lubricant parameter, dimensionless
Z	= number of teeth, dimensionless

Greek Symbols

α	= pressure angle, $^\circ$ (degree)
λ	= specific film thickness, dimensionless
ν	= Poisson ratio, dimensionless
ρ	= specific mass, kg/m^3
η	= kinematic viscosity, m^2/s (cSt)
η_0	= kinematic viscosity of lubricant at atmospheric pressure, m^2/s (cSt)
ζ	= pressure-viscosity coefficient, $1/\text{MPa}$ (in^2/lbf)
μ_{MIC}	= calculated friction coefficient, dimensionless
τ	= shear stress, MPa

σ = normal stress, MPa

Subscripts

x, y, z = relative to directions of cartesian coordinates

1 = relative to running-in step

2 = relative to pitting step

Experimental Procedure

Materials

The material used in the manufacture of spur gears was the AISI 8620 steel. The gears were machined and submitted to heat and thermochemical treatment at Wiser, Pichler & Cia Ltda. The schematic sequence of such treatments is shown in Fig. 4.

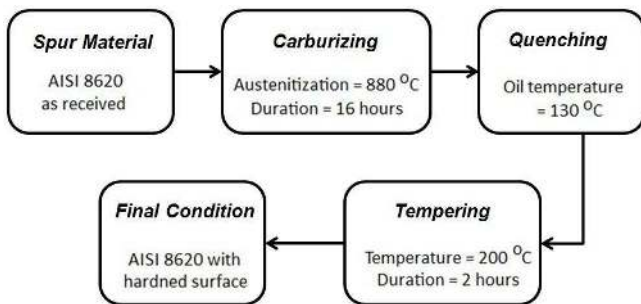


Figure 4. Treatment sequence performed on AISI 8620 steel.

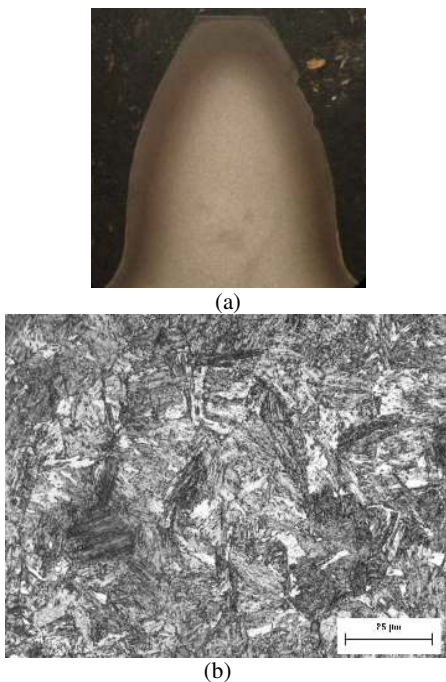


Figure 5. Pinion tooth macro and micrograph: (a) carburized layer, (b) martensitic microstructure.

Figure 5 shows images (macro and micrograph) of one of the teeth after a chemical etching with 5% Nital solution. Fig. 5(a) shows the hardened layer, the thickness of which is in Table 1.

Figure 5(b) shows the AISI 8620 steel microstructure resulting after the heat treatments that formed martensite with some retained austenite. The final layer hardness was 40 HRC.

Table 1. Hardened layer thickness (mm).

Pinion	Wheel	Pinion	Wheel
1.7 ± 0.2	1.5 ± 0.1	1.4 ± 0.1	1.5 ± 0.2

The lubricant used was an ISO VG 100. The gears were dip lubricated with an oil volume of 1.5 liters. After each test step the used oil was removed and replaced by new oil so that the debris generated in the previous step would not influence the pitting formation (by indentation). The main properties of the lubricant are shown in Table 2.

Table 2. ISO VG 100 characteristics in two temperatures.

	Unit	Running-in Step	Pitting Steps
Temperature	°C	60	90
Kinematic viscosity – η	m ² /s (cSt)	39.9 x 10 ⁻⁶ (39.9)	14.6 x 10 ⁻⁶ (14.6)
Pressure-viscosity coefficient – ζ	1/MPa (in ² /lbf)	1.97 x 10 ⁻² (1.36 x 10 ⁻⁴)	1.62 x 10 ⁻² (1.12 x 10 ⁻⁴)
Specific mass – ρ	kg/m ³	855.7	840.0

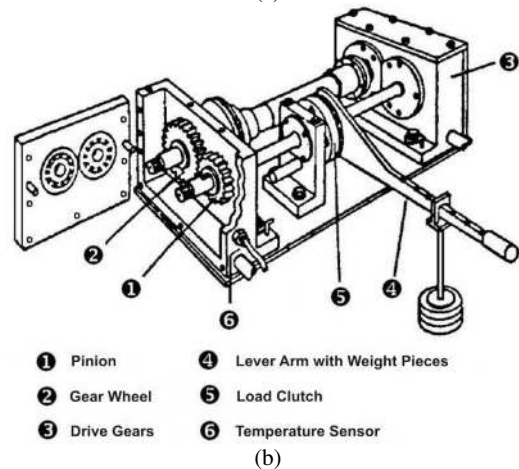
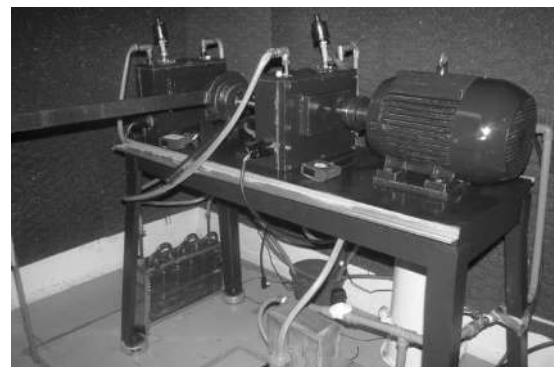


Figure 6. FZG gear test rig: (a) picture and (b) schematic view.

Contact fatigue tests

For the contact fatigue tests it was used the FZG-LASC tribometer. Figure 6 shows an overview of this equipment. This tribometer was designed, manufactured and assembled in the Contact and Surface Laboratory (LASC-UTFPR). By using the power recirculation principle, two pairs of gears can be tested at the same time. The load is imposed on the gears by applying torque on the shaft that the wheel is mounted on (FZG loads k6 and k9). A twist on the wheel axis is achieved by applying an eccentric load, using a lever and dead weight.

Table 3. Gear type C characteristics and AISI 8620 properties.

Parameter	Unit	Pinion	Wheel
Number of teeth – Z	–	16	24
Module – m	mm	4.5	
Center Distance	mm	91.5	
Pressure angle – α	°	20	
Face width – b	mm	14	
Addendum modification	–	+ 0.182	+ 0.171
Addendum diameter	mm	82.45	118.35
Hardness	HRc	40 ± 1	
Young modulus – E	GPa	205	
Poisson ratio – ν	–	0.3	

To produce accelerated wear on the flank of gear teeth, it is common to use gears with modified profile. FZG type-C spur gears were used in the contact fatigue tests, and their characteristics are shown in Table 3.

The gears used as samples were tested in the FZG-machine following a similar procedure proposed by the FZG Institute (FZG, 1992) for pitting testing. In this method, in addition to the geometrical characteristics of the gears, the loading forms for the running-in and pitting test stages are also presented. The loading stages are shown in Table 4.

Table 4. Loading stages and speed used in contact fatigue tests.

FZG load	Stage of test	Wheel speed (rpm)	Torque (N.m)	Contact pressure (MPa)
k6	<i>running-in</i>	1450	135.3	1153.8
k9	<i>pitting</i>		302.0	1723.8

Figure 7 shows the sequence of the methodology used in the contact fatigue experiments in gears. At the end of the tests, each gear (four pairs) was subjected to a 7.5×10^6 -cycle (pinion) and 5.0×10^6 -cycle (wheel) load.

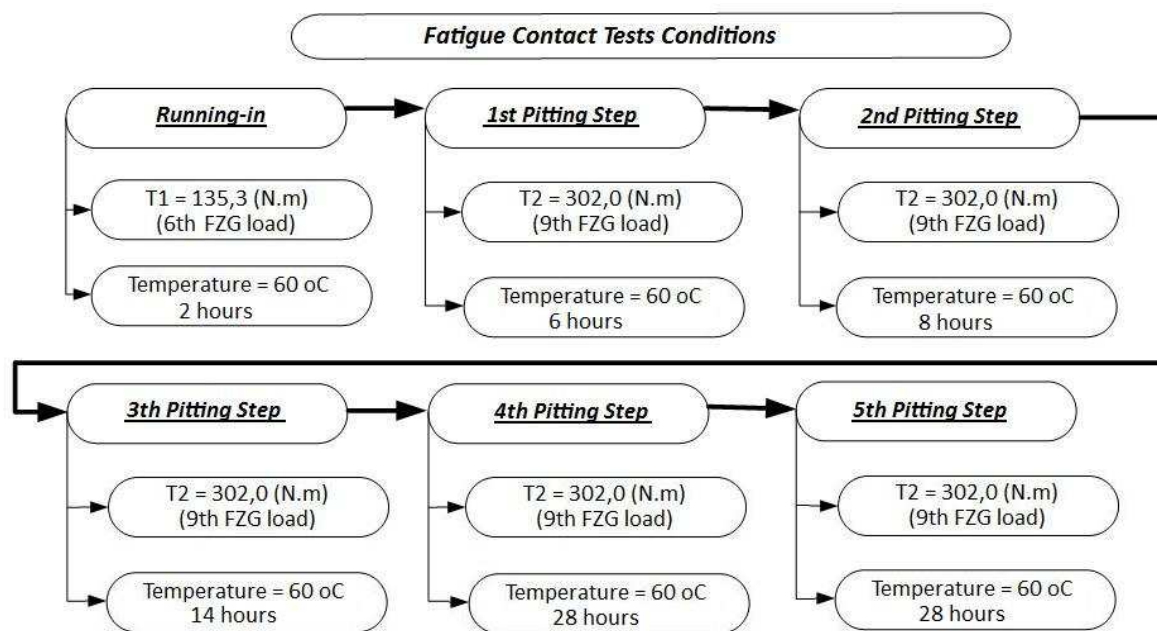


Figure 7. Operating conditions used in the contact fatigue tests.

Damaged by pitting

Macroscopic images were taken from the gear teeth flank, showing the condition before running-in and after each step of the fatigue tests, so that the damage evolution in the flanks with the loading cycles could be observed. These images were used to quantify the pitting area. This procedure was done for all damaged teeth of each gear.

Figure 8(a) shows an image of a pinion tooth flank where it is possible to identify two regions: (1) the effective contact area and

(2) the lateral areas where there is no contact during mesh. Areas with pitting damage identified in Fig. 8(b) are measured using image analysis software. The ratio of the damaged area and the effective contact area reports the percentage of damage on each tooth at each step of pitting test.

The total damage of all the gear teeth was divided by the total active area of all flanks and, in this paper, the resulting value is called average damage percentage. Figure 9 shows an example of the damage evolution in a pinion tooth.

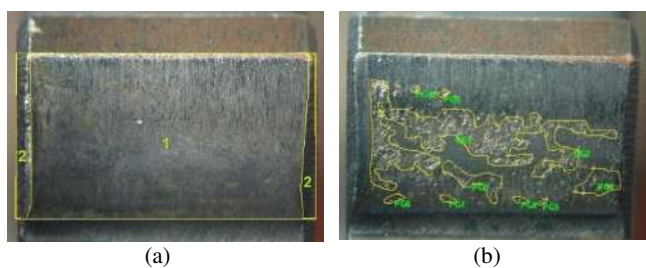


Figure 8. Images of pinion tooth showing the surface aspect (a) before and (b) after pitting test.

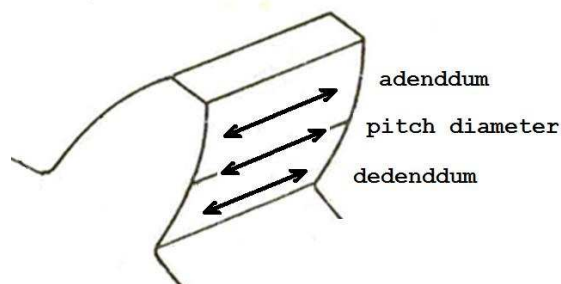


Figure 10. Position of roughness measurement: addendum, pitch diameter and dedendum.

Five teeth of each pinion and wheel were selected randomly. Having the roughness values measured in these teeth, two different types of statistical analysis were performed after each fatigue test: average roughness around the flank (see Table 5) and tooth roughness by region (addendum, pitch diameter and dedendum).

Table 5. Surface finish at the beginning of tests and after the running-in stage.

	Roughness Parameters			
	Milling		Shaving	
	As received	After running-in	As received	After running-in
R_a (μm)	1.57 ± 0.13	0.88 ± 0.14	0.92 ± 0.08	0.51 ± 0.09
R_{vk} (μm)	2.5 ± 0.5	1.51 ± 0.14	1.4 ± 0.2	1.04 ± 0.17
R_{sm} (mm)	0.07 ± 0.01	0.12 ± 0.02	0.04 ± 0.01	0.07 ± 0.01

Table 5 shows that there was a clear roughness reduction after the running-in stage for both kinds of surface finishing (milling and shaving).

Specific film thickness – λ

In EHD conditions, the film variation as a function of local surface roughness is perhaps best characterized by a parameter proposed by Tallian (1967). In Eq. (1) the ratio of the minimum film thickness (h_{min}) to the composite surface roughness of two surfaces in contact is defined as specific film thickness (λ). The parameters R_{q1} and R_{q2} are the root mean square (RMS) roughness values of each surface in contact (pinion-wheel).

$$\lambda = \frac{4}{3} \cdot \frac{h_{min}}{\sqrt{R_{q1}^2 + R_{q2}^2}} \quad (1)$$

Equation (2), proposed by Dowson and Higginson (1977), is used to determine the minimum film thickness.

$$h_{min} = 2.65 R'_{eq} (\zeta \cdot E')^{0.54} \left(\frac{\eta_o U}{E' \cdot R'_{eq}} \right)^{0.7} \left(\frac{P}{b \cdot E' \cdot R'_{eq}} \right)^{-0.13} \quad (2)$$

where P is the transverse load, b is the gear width, U is the average speed, η_o is the kinematic lubricant viscosity (at atmospheric pressure and operating temperature), ζ is the pressure-viscosity



(a)



(b)



(c)

Figure 9. Evolution of damage in a tooth of a machined gear. (a) As received, (b) after the 4th pitting step and (c) after the 5th pitting step.

Roughness

To determine roughness of the gear teeth, measurements were made on the teeth flank in the axial direction (parallel to the gear axis). Figure 10 shows the directions of roughness measurements.

coefficient, R'_{eq} is the equivalent curvature radius (at the point of contact of the teeth) and the effective Young modulus is E' .

Local friction coefficient – μ_{MIC}

To calculate the friction coefficient on the contact path at each point of the flank of gear teeth, it was used the model proposed by Michaelis (Castro and Seabra, 2007), which is shown in Eq. (3).

$$\mu_{MIC} = 0.171 \left(\frac{W_L}{R'_{eq} \cdot V_R} \right)^{0.2} \eta_o^{-0.05} \left(\frac{R_{aEq}}{d_1} \right)^{0.25} X_L X_C \quad (3)$$

In his proposal, Michaelis makes reference to the following parameters: the specific normal load (W_L) in N/mm; the pinion pitch diameter (d_1); the rolling speed (V_R); the equivalent arithmetic average roughness of contact surfaces (R_{aEq}); the correction factor that considers what kind of additives exist in the lubricant (X_L) and the correction parameter for gears that has coated surface (X_C). In this work $X_L = 1$ (additive-free lubricant) and $X_C = 1$ (gears without coated surface).

Along the contact path, several parameters may change on each point of the flank of gear teeth. Listed below are the equations for the evaluation of each parameter that changes along the contact path.

- Equivalent arithmetic average of the roughness of surfaces in contact:
$$R_{aEq} = \left(\frac{R_{a1} + R_{a2}}{2} \right) \quad (4)$$

- Equivalent radius of curvature at the contact point of teeth:
$$R'_{eq} = \left(\frac{1}{R_{1i}} + \frac{1}{R_{2i}} \right)^{-1} \quad (5)$$

- Rolling speed of the gears:
$$V_R = \left(2 + \Gamma_y - \frac{\Gamma_y}{i} \right) \cdot V \cdot \sin \alpha \quad (6)$$

In Eqs. (4), (5) and (6), the relevant parameters are: arithmetic average of the roughness of each tooth (R_{a1} , R_{a2}); tangential speed (V); the gear ratio (i) and the measured dimensionless parameter in contact mesh line (Γ_y). This parameter represents the distance from the pitch point up to the contact point considered.

Contact stress

To calculate the contact stress on the flank of teeth, the analytical solution proposed by Hertz (Norton, 2008) was used. In this solution, the gear contact is analyzed as if the contact was between two cylinders, and is assumed that the radii of these two cylinders are equal to the curvature radius of the teeth in each point in contact. With these assumptions, the contact-patch half-width (a) is then found by Eq. (7).

$$a = \sqrt{\frac{4}{\pi} \cdot \frac{W}{b} \cdot \frac{R'_{eq}}{E'}} \quad (7)$$

A plot of the pressure distribution in the contact zone is depicted in Fig. 11. The contact pressure (p_{max}) is maximum at the center and zero at the edges. The maximum contact pressure can be obtained by Eq. (8).

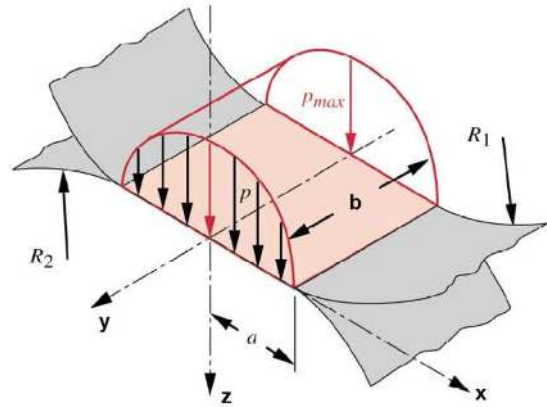


Figure 11. Ellipsoidal-prism pressure distribution and contact zones in cylindrical Hertzian contact (Norton, 2008).

$$P_{max} = \frac{2W}{\pi \cdot a \cdot b} \quad (8)$$

Except to the pitch point, there is the possibility of sliding as well as rolling in all contact points. In the pitch point exists only rolling motion. The tangential sliding force (friction force) causes a significant effect on the stress when compared to the situation where there is only the pure rolling or static pressure.

According to the contact geometry shown in Fig. 11, with the x axis aligned in the direction of motion, z axis in a radial direction of the tooth and the y axis aligned in the axial direction (face width), the stresses at the surface (when $z = 0$) due to the p loading (a normal load) are:

$$\text{if } |x| \leq a \text{ then } \sigma_{xn} = -P_{max} \cdot \sqrt{1 - \frac{x^2}{a^2}} \quad (9)$$

$$\begin{aligned} \sigma_{xn} &= 0 \\ \text{if } x < -a \text{ or } x > a \text{ then } \sigma_{xn} &= \sigma_{zn} \\ \tau_{xzn} &= 0 \end{aligned} \quad (10)$$

The stresses due to the frictional force (a tangential load) at the surface (when $z = 0$ and μ_{MIC} = friction coefficient) are:

$$\text{if } x \geq a \text{ then } \sigma_{xt} = -2\mu_{MIC} \cdot P_{max} \cdot \left(\frac{x}{a} - \sqrt{\frac{x^2}{a^2} - 1} \right) \quad (11)$$

$$\text{if } x \leq -a \text{ then } \sigma_{xt} = -2\mu_{MIC} \cdot P_{max} \cdot \left(\frac{x}{a} + \sqrt{\frac{x^2}{a^2} - 1} \right) \quad (12)$$

$$\begin{aligned} \text{if } |x| \leq a \text{ then } \sigma_{xt} &= -2\mu_{MIC} \cdot P_{max} \cdot \frac{x}{a} \\ \sigma_{zt} &= 0 \end{aligned} \quad (13)$$

$$\text{if } |x| \leq a \text{ then } \tau_{xzt} = -\mu_{MIC} \cdot P_{max} \cdot \sqrt{1 - \frac{x^2}{a^2}} \quad (14)$$

$$\text{if } x < -a \text{ or } x > a \text{ then } \tau_{xz} = 0 \quad (15)$$

The total stresses on each cartesian plane is found superposing the components due to the normal and tangential loads, as shown in Eqs. (16):

$$\begin{aligned} \sigma_x &= \sigma_{xn} + \sigma_{xt} \\ \sigma_z &= \sigma_{zn} + \sigma_{zt} \\ \tau_{xz} &= \sigma_{xzn} + \sigma_{xzt} \end{aligned} \quad (16)$$

For short gears we have a plane stress state and the stresses σ_y , τ_{xy} e τ_{yz} can be neglected.

Results

Running-in stage

The running-in stage aims at equalizing the contact area and stabilizing such parameters as the friction coefficient. Figure 12 shows the friction coefficient along all points of contact during meshing, based on the pinion diameter. It can be observed that, during the running-in test, there is a drop in the friction coefficient for both milling and shave finishes. This fact is related to the reduction of surface roughness of the flank during the tests (see Table 5).

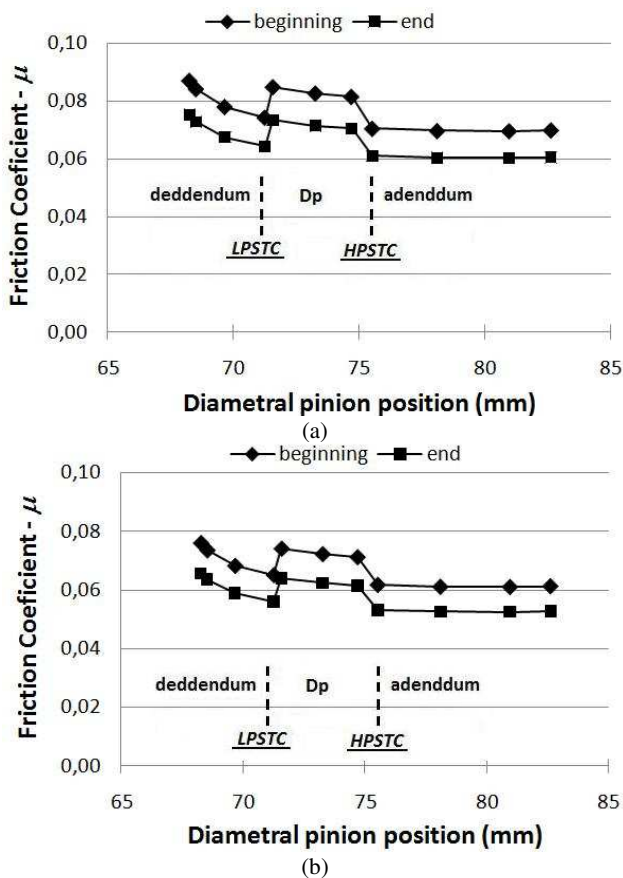


Figure 12. Friction coefficient variation on the contact path. (a) Milling, (b) shaving.

Figure 13 shows the roughness profile measured at the pitch-line region of a shaved gear, before and after the running-in stage. Both the roughness height (R_a) reduction and the increased number of peaks (R_{sm}) lead to the actual growth of the contact area and a local reduction of the stress situation on the surface. Similar results were shown by Cardoso et al. (2009) in nitrided gears lubricated with two ISO VG 100 biodegradable ester fluids with low toxicity additivation.

Figure 12(a) shows that, along the contact path, the friction coefficient presents a decline in the region between the root and the top of the gear. However, it is observed that the friction values show a plateau in the region between the LSPTC and HPSTC points.

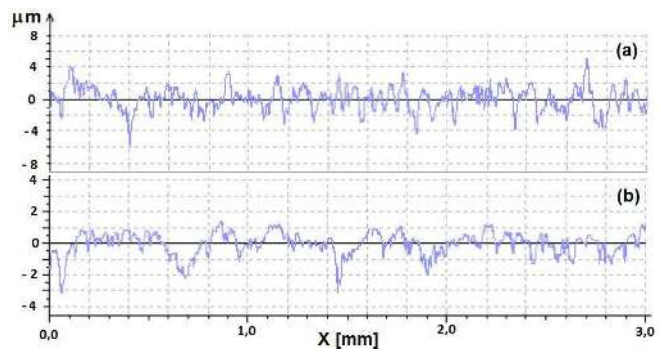
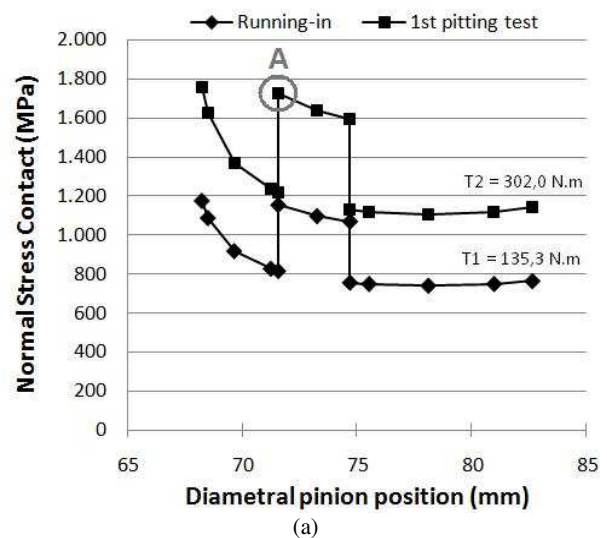


Figure 13. Pinion roughness profiles measured in the axial direction and near the pitch line of tooth with shave finishing. (a) As received, and (b) after running-in tests.

This fact is due to the increased normal load, which is defined by the load sharing function. This load change can be clearly observed in Fig. 14 (a). It also identifies a similar behavior of the contact stresses distribution for the two test conditions. As presented by Krishnamurthy and Rao (1987), the influence of the torque and the presence of high contact stresses in the dedendum region can be observed once again.



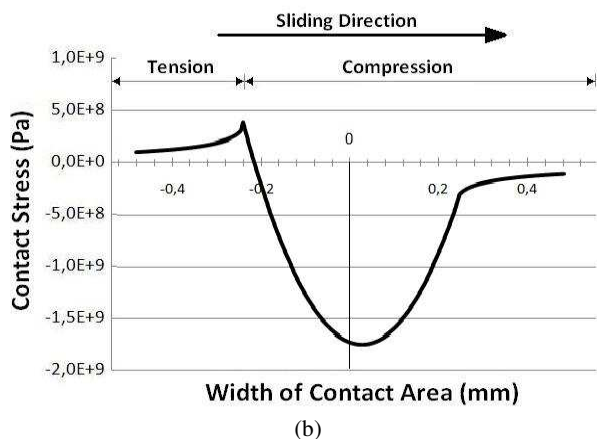


Figure 14. (a) Variation in contact stress on the contact path: running-in (T1) and pitting (T2). (b) Contact stress distribution on apparent contact area (LSPTC of milling pinion at A point).

Figure 14 (b) shows the stress distribution in the apparent contact area at **A** point. It is observed that, due to the friction efforts, the maximum compression stress is shifted into the slip direction.

Tooth flank damaged area

The relation between roughness and contact fatigue resistance was observed by measuring the damage areas. As shown in Fig. 15, milled gears started being damaged during the second pitting stage. From running-in until the 3rd pitting step, the shaved gears did not show any evidence of significant pitting. Therefore, it can be stated that the shaving surface finishing will provide greater resistance to the damage derived from the contact fatigue, especially by delaying the onset of damage.

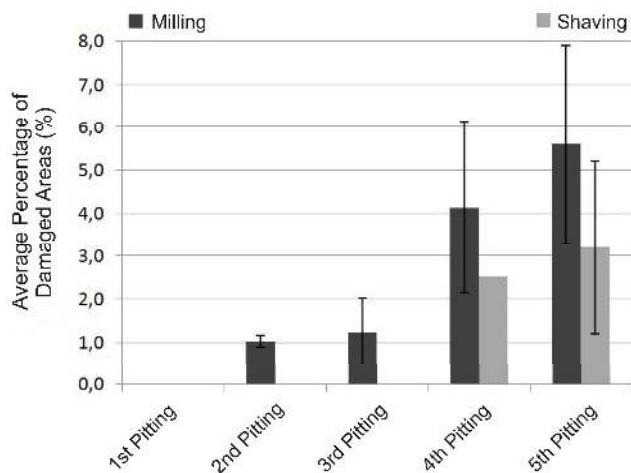


Figure 15. Average damage percentage in gears (pinion + wheel).

Despite the changes in the roughness parameters and friction coefficient during the pitting tests, the values of maximum contact stress do not show significant changes either for the shaving or milling flank finishing. The maximum difference of only 6% (in the pitch line region of milled gears) was found. Figure 16 shows the values of maximum contact stress for the milled gears after the 5th step of pitting test.

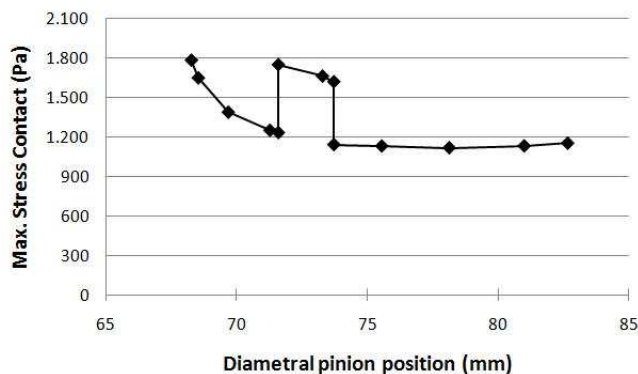


Figure 16. Variation in contact stress on the contact path during pitting steps.

The specific film thickness (λ) at the gears' point of contact is a parameter that might explain the influence of the different surface finishes on the wear of the gears under study. It is observed in Fig. 17 that the specific film thickness is always lower at the milled gears contact, thus making the loading conditions more severe. Analyzing the λ values for all contact conditions it can be stated that the lubrication regime is EHD.

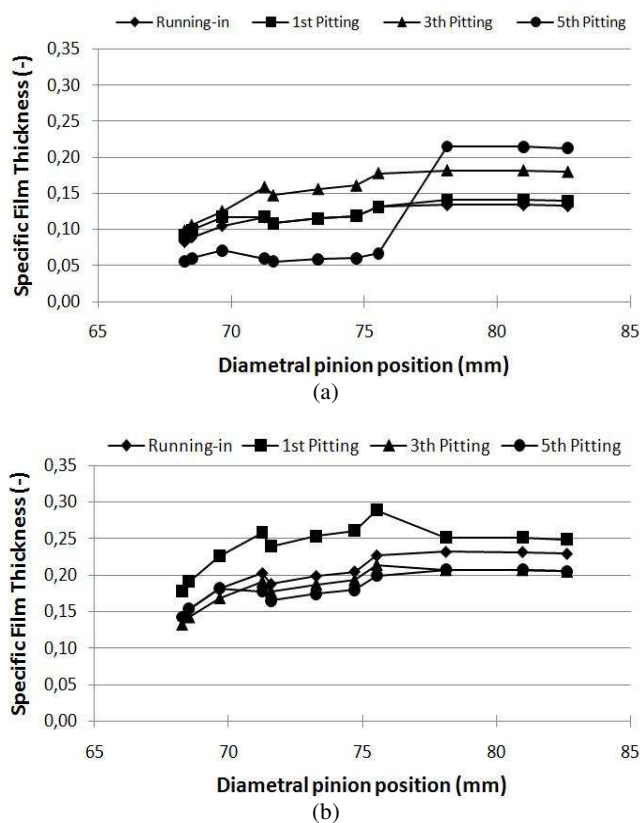


Figure 17. Variation in specific film thickness (λ) stress on the contact path during pitting steps: (a) milling, (b) shaving.

Discussion on wear mechanisms

Due to the kinematic characteristics of the gear teeth contact, the teeth lubricating conditions in addendum, pitch line and dedendum are very different. By observing Fig. 17 with regard to the tooth flank, it can be noticed that at - and below - the pitch-line region, the

lowest specific film thicknesses are in these regions. Adding the fact that this parameter is directly linked to the flank surface finishing situation, it can be stated that the more aggressive the contact conditions, the greater is the occurrence of damage by pitting. Such damages reduce the film thickness even more, thus intensifying the contact severity.

Figure 18 shows the evolution of the R_{vk} roughness parameter, obtained from the measurements made in the tooth flank in axial direction during the pitting tests.

As defined by Magalhães et al. (2007), it is observed that, below the pitch line of milled gears diameter, the R_{vk} parameters increased significantly, indicating the presence of deep valleys, which are related to the presence of pitting on the teeth flanks. This enhancing effect of the loading aggressiveness at the point of contact was not very clear in the shaved gears. However, it is possible to establish a direct correlation of the surface damage evolution (Fig. 15) with both parameters, λ (Fig. 14) and roughness R_{vk} (Fig. 18).

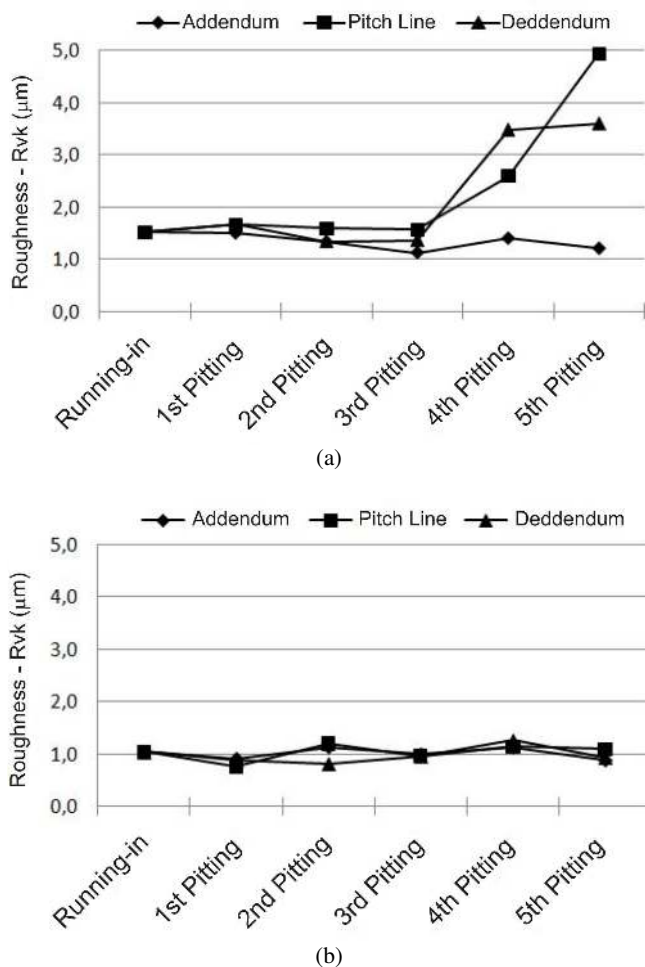


Figure 18. Evolution of R_{vk} roughness parameter during the pitting tests: (a) milling, (b) shaving.

Figure 19 shows the sliding rate at the contact area for the C-type gears test conditions. By comparing the addendum and dedendum regions, it is possible to identify that the sliding rate is higher in the pinion dedendum region. This fact also contributes to a more intense loading severity.

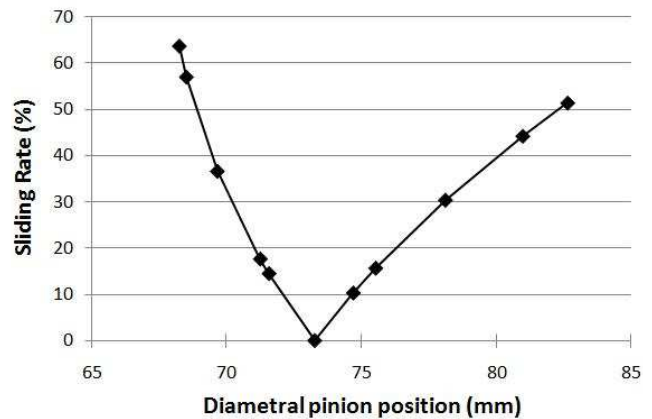


Figure 19. Sliding rate in tooth contact.

Figure 20 shows the surface of a milled tooth pinion after the 5th pitting step. The dedendum region presents wear by pitting and spalling, typical of high stress and low film thickness. In the addendum region, there is a predominance of abrasive wear mechanisms. However, this kind of damage has not been addressed in this work.

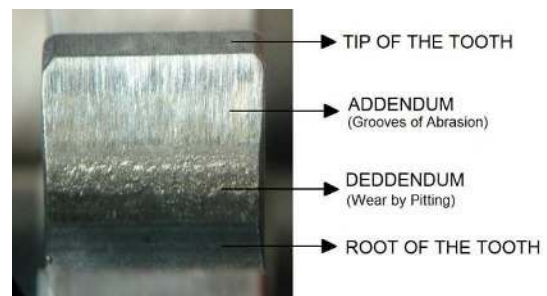


Figure 20. Flank surface of milled pinion after the 5th pitting step.

Conclusions

The results obtained in this work allow the following conclusions:

1. The surface finishing has a strong influence on the origin of contact fatigue damage (pitting and spalling). The gears with shaving showed better wear resistance than milling ones, since they delay the initiation of sub-surface cracks.
2. A more uniform load distribution on the teeth flank, achieved with lower R_a and higher R_{sm} values, leads to increase the wear resistance.
3. The results for the specific film thickness (λ) show that the lubrication regime is severe along the entire contact path for both gear finishes, shaving and milling.
4. The gears manufactured by shaving have higher λ values, i.e., the contact is less severe than that on milled gears, providing a better load distribution.
5. The combined use of the two techniques, monitored by images and roughness measurement at each test step, proved to be very effective in promoting the understanding of the contact fatigue phenomena in gears.
6. The load-sharing function showed to have great influence in the regional deterioration of the teeth flank and may be accompanied by roughness measurements in the axial direction of the gears.
7. The wear mechanisms and the damage morphology, identified by microscopic observation of the tooth surface, show the

importance of surface finish, the level of contact stresses and the lubricant film thickness to wear on gear teeth.

Acknowledgements

The authors would like to express their sincere gratitude to the support from National Scientific and Technological Development Council (CNPq Project 134251/2007-5), Surface Phenomena Lab. (LFS-EPUSP) and the companies: WEG Motores S.A., Wieser & Pichler Cia. Ltda, COSAN (Fuels and Lubricants) and TUPY S.A.

References

- ASM, 1992, "ASM Handbook Volume 18: Friction, Lubrication and Wear Technology", *ASM International*, pp. 535-545.
- Cardoso, N.F.R., Martins, R.C.A., Seabra, J., Igartua, B., Rodriguez, J.C. and Luther, R. D., 2004, "Micropitting performance of nitride steel gears lubricated with mineral and ester oils", *Tribology International*, Vol. 42, pp.77-87.
- Castro, M.J.D., 2004, "Gripagem de engrenagens FZG lubrificadas com óleos base", Doctoral Thesis, Universidade do Porto, Portugal, 323 p.
- Castro, M.J.D. and Seabra, J., 2007, "Coefficient of friction in mixed film lubrication: Gears versus Twin-discs", Proceedings of the Institution of Mechanical Engineers, Part J: *Journal of Engineering Tribology*, Vol. 221, No. 3, pp. 399-411
- Cheng, H.S., 1983, "Elastohydrodynamic Lubrication", in Handbook of lubrication, E.R. Booser, Ed. CRC Pres: Boca Raton, pp. 155-160.
- DIN 3990-4, 1987, "Calculation of load capacity of cylindrical gears; calculation of scuffing load capacity", 22 p.
- Dowson, D. and Higginson, G.R., 1977, "Elastohydrodynamic Lubrication", Pergamon Press, Oxford, 235 p.
- FZG, 1992, "Description of the pittingtest", Institute for Machine Elements – Gear Research Center, 08 p.
- Grubin, A.N., 1949, "Fundamentals of the Hydrodynamic Theory of Lubrication of Heavily Loaded Cylindrical Surfaces", Ed. Translation of Russian Book, No. 30, Central Scientific Institute for Technology and Mechanical Engineering, Moscow, Russian, DSIR London Translation No. 337, pp. 115-166.
- Hohn, B.R. and Michaelis, K., 2004, "Influence of oil temperature on gear failures", *Tribology International*, Vol. 37, pp. 103-109.
- Hutchings, I. M., 1992, "Tribology: friction and wear of engineering materials", Ed. Butterworth – Heinemann, Oxford, pp. 58-76.
- Imrek, H., 2009, "Performance improvement method for Nylon 6 spur gears", *Tribology International*, Vol. 42, pp. 503-510.
- ISO 6336 – 1, 2006, "Calculation of load capacity of spur and helical gears – Part 1: Basic principles, introduction and general influence factors", 109 p.
- Krishnamurthy, S. and Rao, A.R., 1987, "Effect of sursulf treatment on the performance 0.14% C steel gears", *Wear*, Vol. 120, pp. 289-303.
- Magalhães, L., Seabra, J. and Martins, R., 2007, "Austempered ductile iron (ADI) gears: Power loss, pitting and micropitting", *Wear*, Vol. 264, pp. 839-849.
- Norton, R.L., 1998, "Surface Failure" in Machine Design: An Integrated Approach, New Jersey: Prentice Hall, pp. 419-480.
- Stachowiak, G.W. and Batchelor, A.W., 2005, "Engineering Tribology", Elsevier Butterworth-Heinemann, pp. 282-298.
- Tallian, T.E., 1967, "On competing failure mode in rolling contact fatigue", ASLE Transaction, Vol. 10, pp. 418-439.
- Walton, D. and Goodwin, A.J., 1998, "The wear of unlubricated metallic spur gears", *Wear*, Vol. 222, pp. 103-113.
- Winter, H. and Michaelis, K., 1983, "Scoring load capacity of gears lubricated with EP oils", AGMA Technical paper, Fall Technical Meeting, Montreal, Canada, No. 219.17.
- Zafosnik, B., Glodez, S., Ulbin, M. and Flaker, J., 2007, "A fracture mechanics model for the analysis of micro-pitting in regard to lubricated rolling-sliding contact problems", *International Journal of Fatigue*, Vol. 29, pp. 1950-1958.